Smart Structures and Systems, *Vol. 19, No. 1 (2017) 1-10*
DOI: https://doi.org/10.12989/sss.2017.19.1.001

Autonomous evaluation of ambient vibration of underground spaces induced by adjacent subway trains using high-sensitivity wireless smart sensors

Ke Sun[1], Wei Zhang[*1,2], Huaping Ding[3], Robin E. Kim[4] and Billie F. Spencer Jr.[5]

[1]School of Earth Sciences and Engineering, Nanjing University, Nanjing, Jiangsu 210046, China
[2]High-Tech Research Institute of Nanjing University (Suzhou), Suzhou, Jiangsu 215123, China
[3]School of Electronic Science and Engineering, Nanjing University, Nanjing, Jiangsu, 210046 China
[4]Center for Integrated Smart Sensors, KAIST, Daejeon 305-701, South Korea
[5]Department of Civil and Environmental Engineering, University of Illinois at Urbana-Champaign, Urbana, IL 61801, USA

(Received April 5, 2016, Revised October 5, 2016, Accepted October 7, 2016)

Abstract. The operation of subway trains induces secondary structure-borne vibrations in the nearby underground spaces. The vibration, along with the associated noise, can cause annoyance and adverse physical, physiological, and psychological effects on humans in dense urban environments. Traditional tethered instruments restrict the rapid measurement and assessment on such vibration effect. This paper presents a novel approach for Wireless Smart Sensor (WSS)-based autonomous evaluation system for the subway train-induced vibrations. The system was implemented on a MEMSIC's Imote2 platform, using a SHM-H high-sensitivity accelerometer board stacked on top. A new embedded application VibrationLevelCalculation, which determines the International Organization for Standardization defined *weighted acceleration level*, was added into the Illinois Structural Health Monitoring Project Service Toolsuite. The system was verified in a large underground space, where a nearby subway station is a good source of ground excitation caused by the running subway trains. Using an on-board processor, each sensor calculated the distribution of vibration levels within the testing zone, and sent the distribution of vibration level by radio to display it on the central server. Also, the raw time-histories and frequency spectrum were retrieved from the WSS leaf nodes. Subsequently, spectral vibration levels in the one-third octave band, characterizing the vibrating influence of different frequency components on human bodies, was also calculated from each sensor node. Experimental validation demonstrates that the proposed system is efficient for autonomously evaluating the subway train-induced ambient vibration of underground spaces, and the system holds the potential of greatly reducing the laboring of dynamic field testing.

Keywords: underground space; ambient vibration; subway train; wireless smart sensors

1. Introduction

The operation of subway trains induces ground-borne vibration to the surrounding free field (Kurzweil 1979, Chua, Balendra, Balendra *et al*. 1992, Degrande, Clouteau *et al*. 2006, Yang and Hsu 2006), as well as secondary structure-borne vibrations in the constructions within the field (Balendra, Koh *et al*. 1991, Chua, Lo *et al*. 1995, Gupta, Liu *et al*. 2008, Clouteau, Cottereau *et al.* 2013). For the past several decades, urban rail transit has been boomed in developing countries such as China (Qin, Zhang *et al*. 2014). At the same time, a good number of underground constructions, known as underground spaces (Li, Li *et al.* 2013), have also been developed, mostly comprising large shopping malls to attract the passengers. However, these underground spaces are subject to vibration of subway trains, mainly due to their adjacency to the source of the vibration, subway trains. Note that train-induced vibration, along with the associated noise, can cause annoyance and adverse effects on humans, including physical, physiological, and psychological effects (Walker and Chan 1996, Lee and Griffin 2013). Thus, for those peoples who live or work in this specific vibrating environment for long periods of time, assuring that the vibration levels are adequately low is important.

Dynamic field measurements can quantify the ambient vibration effects, verifying the results with either numerical simulation or empirical formula as well (Gupta, Degrande *et al*. 2009). Traditionally, tethered instruments, which require cabling of the transducers with the electrical power and acquisition hardware hubs and central servers, are utilized in measuring subway train-induced ambient vibrations (Degrande, Schevenels *et al.* 2006). By and large, the on-site measurement are often restricted by the cable lengths, to meet the reachable power and communication conditions; the installation cost is determined, to some extent, by the efforts in coping with the cable bundles. Moreover, the tedious centralized raw data processing strategy requires a long time to extract meaningful results.

Wireless smart sensors (WSSs) take advantage of ease of installation, wireless communication, on-board computation, battery power, locally data storage, relatively low cost, and small size (Jo, Sim *et al*. 2012). These features greatly facilitate the dynamic field measurement

[*]Corresponding author, Ph.D.
E-mail: wzhang@nju.edu.cn

http://www.techno-press.com/journals/sss&subpage=8
ISSN: 1738-1584 (Print), 1738-1991 (Online)

operations. For example, the cost and labor required for deploying the transducer and processing raw data can be greatly reduced, compared with those traditional tethered dynamic field testing means. To this end, after several prototypes being developed in the late 1990s, such as Berkley Mote (Kahn, Katz *et al*. 1999) and Stanford WiMMS (Lynch, Law *et al*. 2001), the WSS has received tremendous attention from both academe and industry (Yick, Mukherjee *et al.* 2008). Especially, measuring vibrations using WSSs, in civil structure related academic area, were primarily employed for structural health monitoring purpose for more than a decade. Lynch, Sundararajan *et al.* (2003) firstly validated the field application of the WSS unit using the WiMMS platform. They also implemented the system on the Alamosa Canyon Bridge and measured the acceleration responses to identify the modal properties of the bridge. Kurata, Spencer *et al*. (2005) tested the performance of the Mica mote platform, which is an early type commercial WSS node of Berkeley Mote series. Through free vibration and shaking table tests of a two-story steel structure, they have proved that the Mica Motes show sufficient performance as the wireless sensors to be used for risk monitoring in buildings. Based on the Mica2 of the Berkeley Mote platform, Ruiz-Sandoval, Nagayama *et al.* (2006) developed a high sensitivity acceleration sensor board, Tadeo, whose performance was experimentally validated on a shaking table; the higher resolution and lower noise level of Tadeo allows monitoring of civil infrastructure's low frequency/low amplitude accelerations. Pakzad, Fenves *et al.* (2008) designed an accelerometer sensing board based on the MicaZ platform, for the structural vibration monitoring and modal identification of Golden Gate Bridge, San Francisco, California. Kim, Swartz *et al*. (2010) deployed WSSs using the Narada platform, which is the updated version of WiMMS, on Yeondae Bridge in South Korea; they used WSSs to measure the acceleration responses of the bridge and estimate the bridge mode shapes. Extended from a general-purpose accelerometer (SHM-A) sensor board for the Imote2 platform (Rice and Spencer 2009), an advanced WSS platform developed by Intel research, Jo, Sim *et al.* (2012) developed a high-sensitivity accelerometer (SHM-H) sensor board for measuring low-level ambient vibrations of civil structures. SHM-H was used as a reference sensor in the system identification of a steel truss structure in a laboratory, where the WSS network was consist of several SHM-A and SHM-H sensor boards. The results showed a satisfactory peak capture ability for model shapes under the low-level vibration (1-2 mg range), owing to its excellent capability of capturing low noise level property.

Even though Bennett, Soga *et al*. (2010) employed wireless sensor networks, using the MICAz platform, in the structural monitoring of underground railway environment, they only attained static parameters such as crack displacements and incline angles. So far, few attempts have been made to use WSSs to measure the subway train-induced ambient vibrations in underground spaces. As a matter of fact, the former investigation results have shown that the dynamic characteristics of underground structures

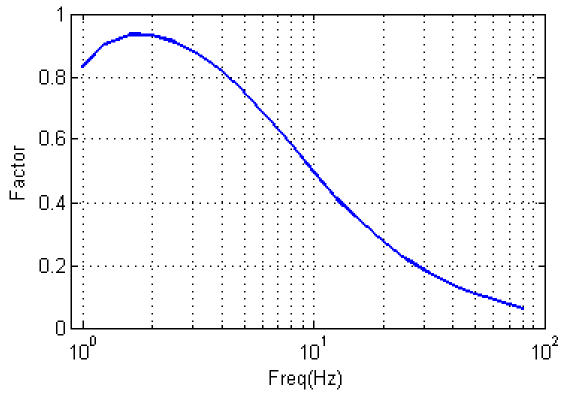

Fig. 1 Frequency weighting w_m (1-80 Hz), with accelerationas the input quantity (ISO 2631-2 2003)

are not identical with those of the superstructures due to the interaction between the underground structure and its surrounding soils (Pitilakis, Tsinidis *et al.* 2014); thus, academic investigations on monitoring subway train-induced ambient vibration deserves to be made.

In this paper, the Imote2 platform, combined with the SHM-H sensor board, was used for developing a WSS-based ambient vibration testing system, especially for autonomous evaluation of the subway train-induced scenario. The proposed system was experimentally validated in a large underground space adjacent to a subway station at Suzhou, China. The vertical vibration responses of the floor slabs, at the interval between the train's arrival and departure, were measured by WSSs. The decentralized on-board computation was implemented; the post-processed distributed vibration levels were directly sent to a central server wirelessly. Subsequently, future analysis on vibration transmission and attenuation behaviors within the floors was performed, by retrieving the processed dynamic signals from the WSSs.

2. Methodology for assessing ambient vibration

When evaluating human response to ambient vibration, the weighted acceleration level, a standardized weighted vibration level, VL, is commonly used (ISO 2631-1 1997). Because of the fact that vibration affecting human's health, comfort, perception, and motion sickness depends on the vibration frequency content, frequency weighting are required to take those frequency differential into account. Thus, VL is quantitatively expressed in terms of decibels, as below

$$VL = 20\lg\frac{a_w}{a_0}\left[dB\right] \tag{1}$$

where a_0 is the reference acceleration amplitude, equaling to 10^{-6} m/s^2; a_w is the measured weighted acceleration root-mean-square (R.M.S.), calculated as the following

$$a_w = \left[\sum_i \left(w_i a_i\right)^2\right]^{\frac{1}{2}} \tag{2}$$

where w_i is a frequency weighting coefficient of the i-th one-third octave band, as shown in Fig. 1. The figure illustrates frequency weighting, w_m, which is in one-third octave bands and applicable where the posture of an occupant does not need to be defined (ISO 2631-2 2003). a_i is the R.M.S. acceleration for the *i*-th one-third octave band, which yields

$$a_w = \left[\sum_i \left(w_i a_i \right)^2 \right]^{\frac{1}{2}} \tag{3}$$

Herein, f_1 is the lower cut-off frequency and f_2 is the upper cut-off frequency; $G(f)$ is the spectral density function, which can be obtained from the Fourier spectrum of the measured acceleration.

3. The autonomous evaluation system

3.1 Requirements and performance

The former investigation reported that the frequency range of interest for subway induced vibrations in buildings is 1-80 Hz (ISO 2631-2 2003). Thus, to be able to capture the frequency contents, an wireless accelerometer needs a sampling rate greater than 160 Hz (Widrow 1956); meanwhile, the published data also revealed that a measuring accuracy of 1 mg, as well as a resolution of 0.05 mg, is necessary for capturing low-level ambient vibrations (Gupta et al. 2009, Degrande et al. 2006, Sanayei et al. 2013).

The SHM-H sensor board, developed from the University of Illinois at Urbana-Champaign, is a high-sensitivity accelerometer board addressing such rigorous requirements. The SHM-H sensor board provides flexible and highly accurate user-selected sampling rates by using a Quickfilter chip, QF4A512, which is a four-channel, 16-bit analog to digital converter (ADC), with programmable digital filters (Jo, Sim *et al*. 2012). Particularly, a low-noise and high-sensitivity MEMS accelerometer, Silicon Designs SD1221L-002, was embedded on the board to measure the acceleration in z-axis. The sensor performance of SD1221L-002 accelerometer, is summarized in Table 1. As can be seen, the maximal resolution of the sensor is 0.043 mg, with a limit of the input range being ± 0.2 g (Jo, Sim *et al*. 2012). Also, the frequency response is 0~400 Hz, which satisfies the frequency range of interest. Other specifications also include a sensitivity of 2 V/g and a noise floor of 5 ug/$\sqrt{Hz}$.

3.2 WSS node configuration

A WSS leaf node (Sim, Li *et al*. 2014), deployed for the on-site acceleration measurement, is composed of a SHM-H sensor board, an Imote2 platform, and a IBB2400CA battery board, As can be seen in Fig. 2(a), each of those modules are stacked via external connectors,. Also, the battery board is embedded in a U-shaped steel base, which is used for mounting the node on the test object.

The Imote2 is a high-performance wireless smart sensor platform, having Intel's low-power X-scale micro-controller processor (PXA271) running at 13-416 MHz and an MMX DSP Coprocessor, along with 256 kB SRAM, 32 MB Flash memory and 32 MB SDRAM, which enables storing longer measurements, as well as the powerful on-board computation capability (Jang, Sim *et al*. 2010). In addition, the integrated wireless transceiver CC2420 radio chip, in the Imote2 is composed of a radio frequency (RF) modem and an antenna, allowing the node to transfer data to the gateway wirelessly.

The IBB2400CA battery board powers the Imote2 using three 1.5-volt batteries. Due to the nature of short-term measurement in this scenario, the power consumption is not of great importance as that is in the long-term health monitoring.

The gateway node (Sim, Li *et al*. 2014), as shown in Fig. 2(b), consists of an Imote2 stacked on an IIB2400 interface board connected to a laptop/tablet PC via USB port. The communication between the leaf node and the gateway node employs the IEEE 802.15.4 wireless protocol standard which has been explicitly for low-power, low data rate wireless sensor networks (LAN/MAN Standards Committee 2003).

Table 1 SD1221L-002 accelerometer specifications

Input Range *g*	Resolution *mg*	Frequency Response H_Z	Sensitivity *mV/g*	Noise Floor $ug/\sqrt{Hz}$
±0.2	0.043	0~400	2000	5

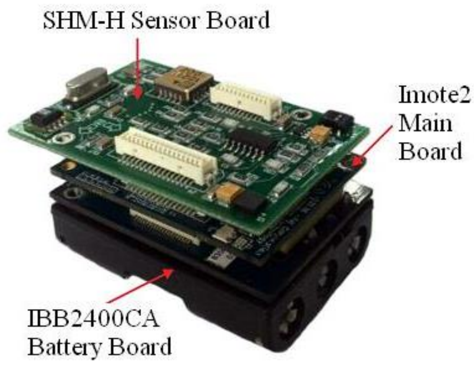

(a) Leaf node

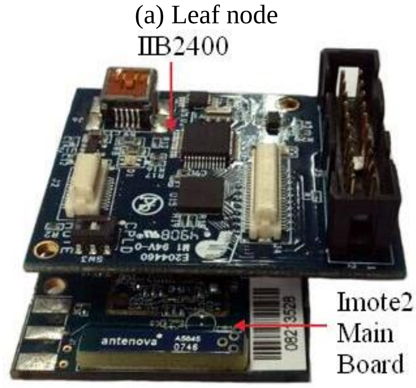

(b) Gateway node

Fig. 2 Layout of the WSS leaf node and gateway node

As for the radio communication, an antenna is designed to be integrated into the Imote2 board, which offers a peak gain of 1.8 dBi. The ordinary radio communication range reaches 50 m in the case of no barrier between two nodes. An external antenna, Antenova Titanis 2.4 GHz Swivel SMA antenna, for example, is optional for the enhancement of the radio communication capability, and the range could be extended up to 300 m without any barrier.

3.3 Embedded vibration level calculation

The embedded software in the WSS node is developed based on the Illinois Structural Health Monitoring Project (ISHMP) Services Toolsuite, version 3.1.0, which implements key middleware functionality to provide high-fidelity measured data and to reliably transmit the data to the base station wirelessly across the sensor network, as well as a library of numerical algorithms. The open-source software, written in NesC language and designed to operate in TinyOS is available at http://shm.cs.uiuc.edu/software.html (Jang, Jo *et al*. 2010). The software can be categorized into a number of different components: network operation, data collection, data processing and power management, et al.. In this paper, one of the network operation application, RemoteSensing, is used to organize network topology and control data stream. The data is sampled at user selectable frequency and duration. The data can be post-processed in each node owing to its on-board computational capability, which includes data compression, fast Fourier transform (FFT), and power spectrum density (PSD). Note that primary windowing functions, such as Hanning, Hamming and Kaiser windows, have also been embedded in the computational core. A pre-test should be done and the obtained signals are manually analyzed to select the proper windowing functions and set it in the core. The power management implements efficient power control using several strategies, such as short-term and long-term sleep modes, triggering only selected nodes that are responsible, and periodical network monitoring (Jang, Jo *et al*. 2010). However, an application for assessing the level of ambient vibration using on-board computational functionalities has not been realized before. Thus, a new data processing application, named VibrationLevelCalculation, has been developed for the on-board computation of the ambient vibration level, collaborating with the other existing components. The implementation of VibrationLevelCalculation is based on previously described vibration level calculation equations.

3.4 Independent data processing strategy

Unlike the centralized data processing strategy used in the traditional tethered systems, independent data processing strategy (Zhou and Yi 2013) can be employed in the WSS network system. With all the necessary algorithms embedded in the computational core, distributed computing can be executed on each WSS leaf node, independently without having to communicate with each other. At first, the central server sends commands to activate the leaf nodes, establish a wireless sensor network (WSN), and set the measurement parameters. Then, after time synchronization, the WSSs start collecting data. The measured data is firstly processed locally by the microprocessor on the Imote2. After that, the brief results, such as the vibration level, FFT and PSD, et al., are wirelessly transmitted from the leaf nodes to the gateway node, which is connected to the central server. If necessary, the raw data stored on the leaf nodes as a flash memory can be retrieved later (Jang, Jo *et al*. 2010) and processed offline on the central server for the fine analysis. Within the entire process, handshaking protocols are used for commands or data being sent to the designated WSS nodes. Fig. 3 illustrates the schematic of the whole system.

4. Experimental validation

4.1 Background

The system was validated in the Xinghai Square, a two-storied large underground space adjoining Metro Line 1 in Xinghai station of Suzhou City, China. The underground space is comprised of two reinforced concrete frame structures, seamlessly standing on both sides of the subway station. The total cover area is 54,511 m^2 and the maximal bury depth is 13.7 m underground. As illustrated in Fig. 4, the rooftop of the underground space is made for the Sunken plaza; the Basement 1, B1, is department stores; the Basement 2, B2, is the parking garage. As seen, the distance, from the side wall of the underground space to the central line of the subway rails is only 10 m. Such a short distance can influence people in the underground space due to the subway train's operation. Along with aforementioned floor plans, the strata enclosing the underground space are also depicted in Fig. 4. Besides, Table 2 lists the physical and mechanical indices of the soils.

The subway trains are all comprised of type B car-body, manufactured by CSR Nanjng Puzhen Co., Ltd. The organization of the compartments is the 4-section-marshalling, Tc+Mp+Mp+Tc, where Tc is the trailer, with a length of 22 m; Mp is the compartment, with a length of 19 m.

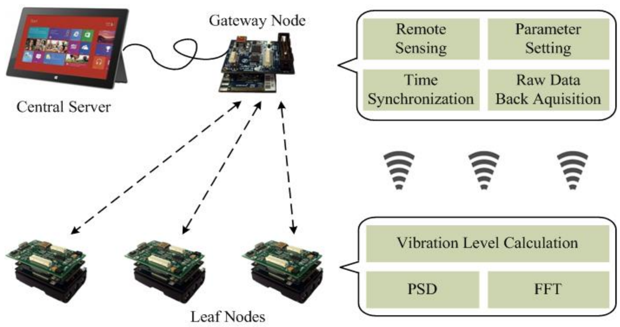

Fig. 3 Schematic of the WSS autonomous evaluation system

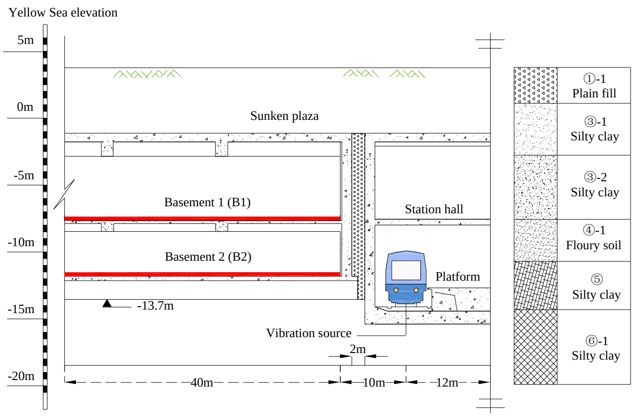

Fig. 4 Sectional view of the measuring site

Table 2 Physical and mechanical indices of soils

Soil layer	ω (%)	γ (KN/m^3)	e	α (MPa^{-1})	E (MPa)	c (KPa)	φ (^{o})
①-2	32.1	1.97	0.650	0.10	16.2	10	31.4
③-1	35.4	1.85	1.005	0.46	4.62	34	10.7
③-2	23.1	1.97	0.679	0.14	12.5	9	30.9
④-1	12.2	2.05	0.465	0.11	13.8	10	33.8
⑤	16.4	2.03	0.578	0.12	11.3	9	27.9
⑥-1	18.1	2.00	0.592	0.15	10.9	12	31.3

The diameters of both Tc and Mp are 2.8 m; the heights of those are 3.8 m; the wheel-spans of those are 1.5 m; the space between two compartments is 0.8m; the total weight of the train marshalling is 127.6 t. In addition, the maximal travelling speed is 80 km/h; the average speed of the train in the interval tunnel is about 50 km/h; the acceleration when arriving or departing is about 1 m/s^2 and the duration between the arrival and departure lasts about 20 seconds. The metro line is paved with integrated unballasted bed.

One WSS leaf node, one WSS gateway node and a laptop were used to set up the field testing system referred above. The leaf node was mounted upon a steel U-shape base, which was firmly fixed onto the floor slab using epoxy. The central server, as well as the gateway node, was placed less than 50 m to both leaf nodes without any barrier in between. The sampling rate was set as 280 Hz and the NFFT as 1024.

The measurement, following the procedure of ISO 5348 (1998), was performed in the basement 1 (B1) and basement 2 (B2), respectively. The layouts of the measure points of B1 and B2 are identical, which are depicted in Fig. 5. As shown, the testing area is square shaped, 40 m by 40 m. The north side wall is close to the subway rail. In total, 39 measurement points were identified along 5 vertical lines, as following: line A is close to the subway station entrance; line C is at the center of the platform; line E is close to the exit; line M and N are in the middle of lines A-C and C-E, respectively. Note that the underground space was just put into service, so that little ambient vibration noise, compared with the subway train-induced ambient vibration, was made by the people or the facilities. In the meanwhile, the test duration was arranged at the low ebb of the subway operation, so that the weight variation caused by the passages on board can be minimized.

4.3 Signal characteristics analysis

The measurements were conducted during the train's arrival-stay-departure period. At each point, 5 sets of measurements were performed. Once the measurement is completed, the results, such as *VLz*, PSD et al., of the measure points was autonomously computed by the leaf node's microprocessor and sent to the central server. After that, the raw data were retrieved from the leaf nodes and post-processed on the central server. The trend term and the noise were trimmed by using the least square method, and then the acceleration time-history spectrum was obtained. Note that Hanning window was pre-chosen and set to minimize the signal leakage errors in FFT.

Taking the B1 floor as an example, Fig. 6(a) depicts the time-history acceleration acquired from measure point E0, during the whole process of the subway-train's arrival-stay-departure. 5 sections are extracted from the spectral. Section 1, 3 and 5, abbreviated as S1, S3 and S5, respectively, all last for 3 seconds. S1 is the typical acceleration signals right before the subway train's arrival; S3 is the ones during the subway train's staying at the platform; S5 is the ones right after the subway train's departure. In addition, section 2 (S2), lasting for about 12 seconds, is the acceleration signals when the subway train arrives; while section 4 (S4), lasting for about 9 seconds, is the ones when the subway train departs. The PSDs of S1 to S5 were obtained by FFT on the central server, as shown in Figs. 6(b)-6(f). As seen, a low frequency peak at 1.64 Hz occurs in all of Figs. 6(b), 6(c), 6(e) and 6(f). Meanwhile, the high frequency peaks vary in the above figures, the ones of Figs. 6 b) and 6(f) both occurring at 62.89 Hz, the one of Fig. 6(c) occurring at 65.63 Hz and, the one of Fig. 6(e) occurring at 72.19 Hz.

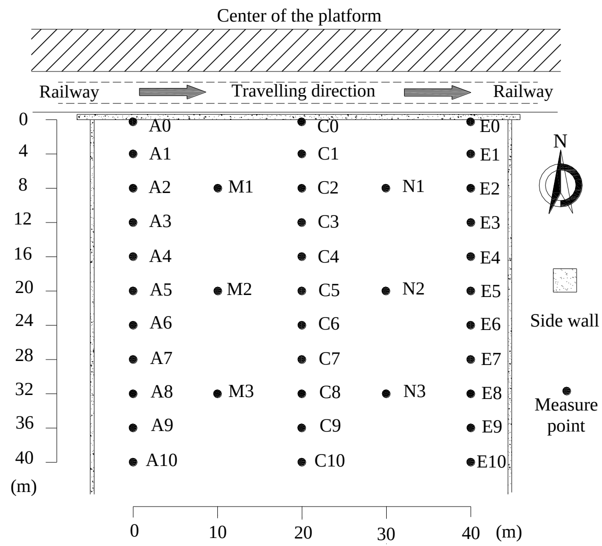

Fig. 5 Measure point layout

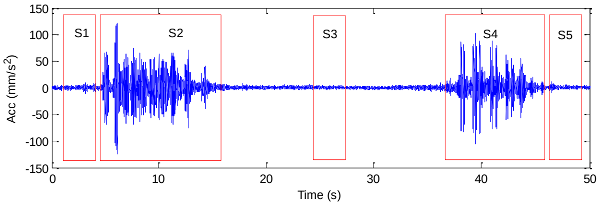

(a) Time-history response

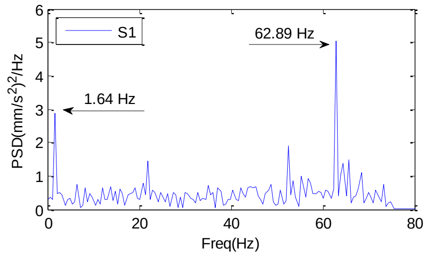

(b) PSD of S1

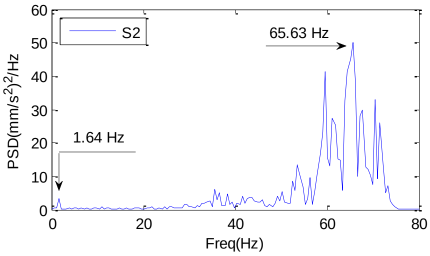

(c) PSD of S2

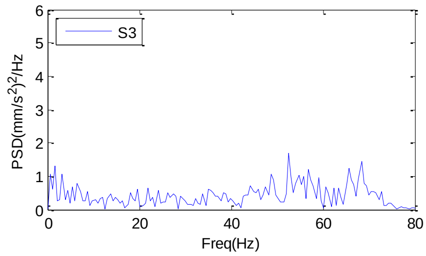

(d) PSD of S3

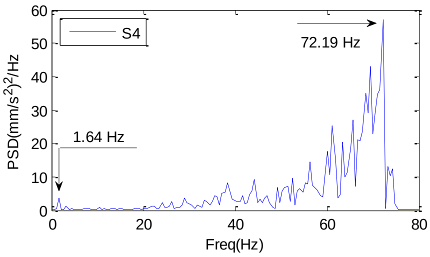

(e) PSD of S4

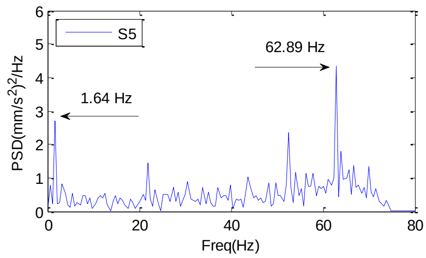

(f) PSD of section 5

Fig. 6 Signal characteristics of E0 of B1

The subway train is electrified, which is powered by the electric traction supply system. So, note the above low and high frequency peaks do not distinctly appear in Fig. 6(d), suggesting that no domain excitation source existing when the subway train stays at the platform. Therefore, we may infer that the 1.64 Hz low frequency is one of the excited natural frequencies of the concrete floor slab. Also, both high frequencies of 62.89 Hz, occurring right before the train's arrival and after the train's departure, should be excited by the running train owing to the travelling wave effect (Sugiyama, Maeda *et al*. 1990). In addition, rich constitution at the high frequency range only exhibit at S2 and S4, suggesting that the power of high frequency attenuates and been absorbed when the elastic waves are travelling in the floor slab, which may also account for the higher frequency's shifting from the higher values to 62.89 Hz. As for the difference of the highest peak frequencies between the train's arrival and departure, namely the 65.63 Hz and 72.19 Hz, different acceleration or deceleration behaviors and the interaction mechanisms between the wheels and the rails may account for it (Zhai 2015).

4.4 Vibration level (VLz)

The value of *VLz* of the measure points was autonomously computed by the leaf node's microprocessor and sent to the central server before the next measurement processing. The values of the *VLz* from the same point were averaged, on the central server, as the representative value of this point. Figs. 7(a) and 7(b) depict the contour maps of the distribution of the vibration level *VLz* of B1 as the train arrives and departures, respectively. As can be seen, Figs. 7(a) and 7(b) exhibit almost the same overall distribution trends. The top-right corner exhibits the maximal *VLz* of 75 dB; the top-left corner exhibits the second maximal *VLz* of 73 dB; the bottom-center exhibits the minimal *VLz* of 65 dB compared with the other spots having the same distance to the side wall. As for the *VLz* along vertical direction, its attenuation along the distance from the top sidewall was quite visible. The maximal attenuation amplitude reached 10 dB, from the near end to the far end of the top side wall. Beyond that, amplification region of *VLz* can be found on measure points of both A6 and E6, with the distance of about 24 m to the top side wall. The contour maps of the *VLz* distribution of B2 at the train's arrival and departure are illustrated in Figs. 8(a) and 8(b), respectively. Also, both contour maps display quite similar trends as those in Figs. 7(a) and 7(b). Only that the maximal *VLz* at the top-right corner is lower to 73 dB. In addition, the regions with the less *VLz* values occur more in Figs. 8(a) and 8(b).

Referring to the national standards of China (JGJ/G170 2009), the maximal allowable peak value of *VLz* should not be greater than 75 dB in the morning or 72 dB at night. The representative values of *VLz*, at top-right corner of B1, just reach the limitation in the morning. Additionally, both top corners of B1 and the top-right corner of B2 had the representative values of *VLz* exceeding the limitation at night. These evaluation results suggest that the ambient vibration effect might do harm to the people if they stay in aforementioned spots of B1 and B2 for a long term.

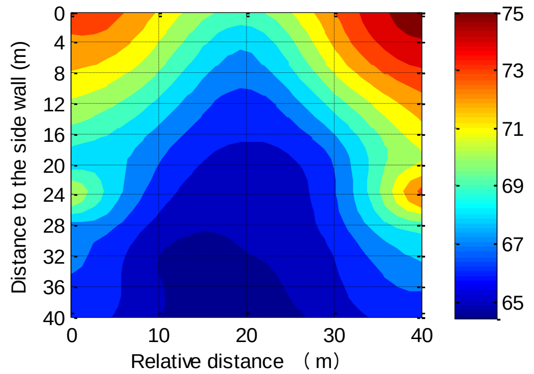

(a) Train arrival

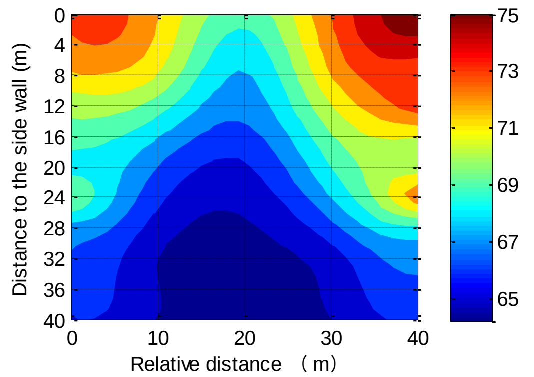

(b) Train departure

Fig. 7 Contour map of *VLz*s of B1

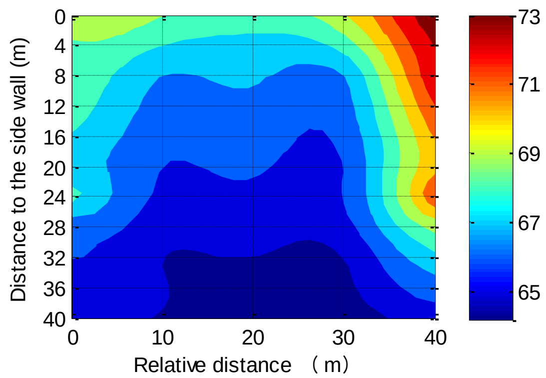

(a) Train arrival

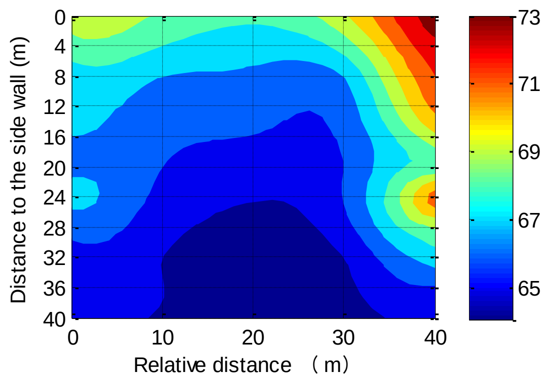

(b) Train departure

Fig. 8 Contour map of *VLz*s of B2

4.5 Discussions

Fig. 9 illustrates the variation trends of the averaged acceleration peak amplitudes along line E, for arrival and departure, respectively. As can be seen, the arrival vibration is a little higher than the departure's, note that strong friction exists between the wheels and the rails as the train brakes for deceleration in arrival, but such strong friction does not exist when the train departs. Basically, both acceleration-peak amplitudes attenuated with the increasing of the distance to the North sidewall. Particularly, at the distance of 12 m, both peak amplitudes enhanced compared with the global trends of attenuation. The similar trend applied to the other measure lines, suggesting an obvious damping effect exists when the elastic waves transmit within the reinforced floor slabs.

Fig. 10 compared the acceleration peak amplitudes of measurement points from line A, C, and E of B1. As can be seen, for both train arrival and departure, the acceleration peak magnitude of line E were the highest; those of line A were in the second highest; those of line C were the least. As referred in section 4.1, the locations of line E and A correspond to the front trailer and tail trailer, respectively, and the location of line C corresponds to the compartment. Note that the friction and bumping actions between the wheels and rails of the trailers are remarkably stronger than those of the compartments, which explains the reason why the acceleration peak magnitudes of line E and line A are greater than that of line C. Moreover, because the power is exerted on the front trailer, line E exhibits the greatest response. Also, note that the vibration level is the logarithm result of the acceleration values, as referred in section 2, so that Fig. 10 exhibit a slightly different trend to Fig. 7 after the logarithm transformation.

As a matter of fact, human's sense varies to different vibration frequency components (ISO 2631-1 1997), which, in turn, influence human health in various degrees. Herein, to investigate the vibrating influence to the human body, the frequency spectra was transformed to one third octave band by using the WSS leaf nodes' microprocessors, and the wm curve in Fig. 1 was used for weighting. Then, the *VLz* on each center frequency (ISO 2631-2 2003) was calculated, using Eqs. (1)-(3), and the results were transmitted to the central server. Fig. 11(a)-(b) plot the one third octave bands at measure point E0 of B1 when the train arrives and departs, respectively. Besides, Figs. 12(a) and 12(b) plot the one third octave bands at measure point E0 of B2.

Figs. 11 and 12 exhibit the similar trends. All of the example *VLz*s are less than 55 dB as the frequency is between 1 and 20 Hz; the *VLz*s increase when the frequency extends from 20 Hz to 80 Hz, almost approaching 75 dB. Noting that the natural frequencies of human parts are mostly less than 20 Hz (Griffin 2012), we may infer that all the vibration components may do less harm to human body as their *VLz*s are small enough. Nevertheless, regarding the durability and the normal service condition of the facilities of the underground space, the region having a total *VLz* greater than the standard criteria should still be controlled. Previous investigation indicates the speed is a critical factor influencing the intensity of train-induced vibration. The main reason relies on the fact that the interaction between the wheels and rails is correlated to the train speed (Zhai 2015). Therefore, slowing down the train's speed in advance on arrival period, or delaying on departure period, are both good options for lowering the ambient vibration induced by subway train operation. Another option is to use low vibration and noise track structure, such as floating slab or elastic fastener, to dissipate high frequency vibration energy, as such to reduce the ambient vibration in adjoining underground spaces.

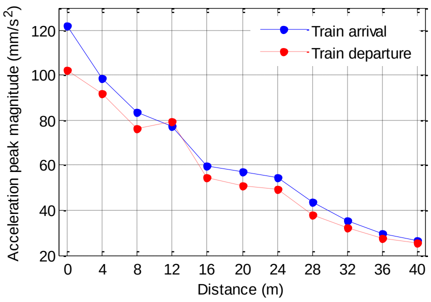

Fig. 9 Variation trends of acceleration-peak amplitudes on line E

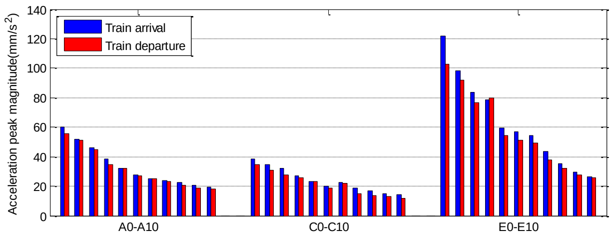

Fig. 10 Comparison of acceleration-peak magnitude of measure points on B1

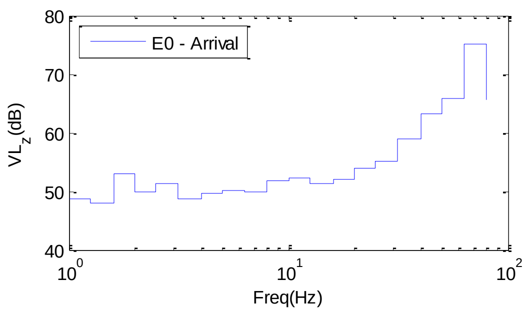

(a) Train arrival

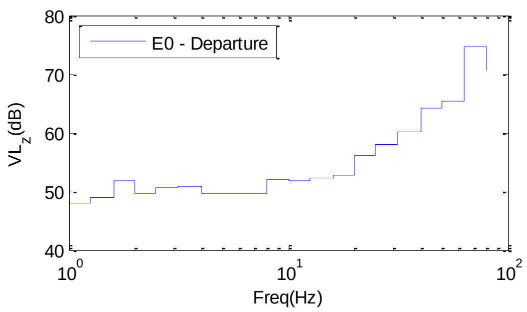

(b) Train departure

Fig. 11 Example VL_Zs by one-third octave band of B1

5. Conclusions

An autonomous measurement and evaluation system for ambient vibration using wireless smart sensors (WSS) were presented in this paper. The system was developed using the Imote2 platform, with an SHM-H high-sensitivity accelerometer board installed on the top. The numerical algorithms for obtaining the weighted acceleration level, defined by ISO standards, were programmed as a new embedded application VibrationLevelCalculation, implemented in the existing algorithm library of the open-source ISHMP Services Toolsuite. An independent data processing strategy is used for the testing, with distributed computation executed on each WSS leaf node. Only processed results, such as the vibration level *VLz* and PSD, were wirelessly transmitted from the leaf nodes to the gateway nodes and the central server. If necessary, the raw data, which has been stored in on-board flash memory, can be retrieved and further processed and visualized offline.

Field tests were conducted using the developed system on a large underground space adjoining a subway station. The vibration level along the z-direction, *VLz*, was autonomously computed on the leaf nodes' microprocessors and sent wirelessly to the central server. Also, both the raw data of the acceleration time-history and the frequency spectrum can be retrieved from the leaf nodes and be further analyzed on the central server. Moreover, spectral vibration levels at one-third octave bands can be acquired after the embedded computation, which is used to assess the vibration influence on human health. The efficacy of the system has been shown, and the potentials of autonomously evaluating subway train-induced ambient vibration in underground spaces have been demonstrated.

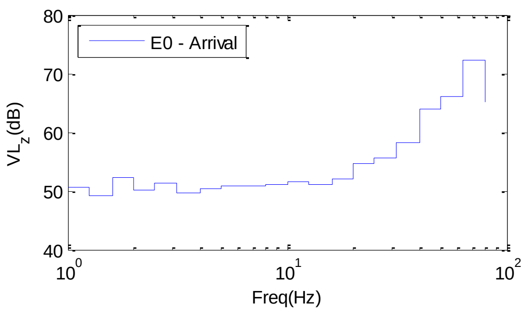

(a) Train arrival

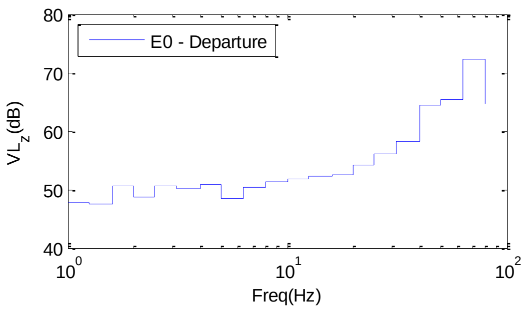

(b) Train departure

Fig. 12 Example VL_Zs by one-third octave band of B2

Acknowledgements

This study is financially supported by National Science Foundation of China (grant No. 40902076), Natural Science Foundation of Jiangsu Province (grant No. BK20141224) and Science & Technology Program of Suzhou (grant No. SYG201318).

References

Balendra, T., Koh, C.G. and Ho, Y.C. (1991), “Dynamic response of buildings due to trains in underground tunnels”, *Earthq. Eng. Struct. D*., **20**(3), 275-291.

Bennett, P.J., Soga, K., Wassell, I., Fidler, P., Abe, K., Kobayashi, Y., and Vanicek, M. (2010), “Wireless sensor networks for underground railway applications: case studies in Prague and London”, *Smart Struct. Syst*., **6**(5-6), 619-639.

Chua, K.H., Balendra, T. and Lo, K.W. (1992), “Groundborne vibrations due to trains in tunnels”, *Earthq. Eng. Struct. D.*, **21**(5), 445-460.

Chua, K.H., Lo, K.W. and Balendra, T. (1995), “Building response due to subway train traffic”, *J. Geotech. Eng.*, **121**(11), 747-754.

Clouteau, D., Cottereau, R. and Lombaert, G. (2013), “Dynamics of structures coupled with elastic media—a review of numerical models and methods”, *J. Sound Vib.*, **332**(10), 2415-2436.

Degrande, G., Clouteau, D., Othman, R., Arnst, M., Chebli, H., Klein, R. and Janssens, B. (2006), “A numerical model for ground-borne vibrations from underground railway traffic based on a periodic finite element–boundary element formulation”, *J. Sound Vib*., **293**(3), 645-666.

Degrande, G., Schevenels, M., Chatterjee, P., Van de Velde, W., Hölscher, P., Hopman, V. and Dadkah, N. (2006), “Vibrations due to a test train at variable speeds in a deep bored tunnel embedded in London clay”, *J. Sound Vib.*, **293**(3), 626-644.

Gupta, S., Degrande, G. and Lombaert, G. (2009), “Experimental validation of a numerical model for subway induced vibrations”, *J. Sound Vib.*, **321**(3), 786-812.

Gupta, S., Liu, W.F., Degrande, G., Lombaert, G. and Liu, W.N. (2008), “Prediction of vibrations induced by underground railway traffic in Beijing”, *J. Sound Vib.*, **310**(3), 608-630.

ISO 5348. (1998), “Mechanical vibration and shock-Mechanical mounting of accelerometers”, *ISO Standard*.

ISO2631, S. I. (2003), “Mechanical vibration and shock-evaluation of human exposure to whole body vibration Part 2: Continuous and shock induced vibration in buildings (1-80 Hz)”, *ISO Standard.*

ISO2631, S.I. (1997), “Mechanical vibration and shock: Evaluation of human exposure to whole-body vibration. Part 1: General requirements”, *ISO Standard*.

Jang, S., Jo, H., Cho, S., Mechitov, K., Rice, J.A., Sim, S.H. and Agha, G. (2010), “Structural health monitoring of a cable-stayed bridge using smart sensor technology: deployment and evaluation”, *Smart Struct. Syst.*, **6**(5-6), 439-459.

JGJ/G170 (2009), “Standard for limit and measuring method of building vibration and secondary noise caused by urban rail transit”, *Industry Standard of People's Republic of China*.

Jo, H., Sim, S.H., Nagayama, T. and Spencer Jr, B.F. (2011), “Development and application of high-sensitivity wireless smart sensors for decentralized stochastic modal identification”, *J. Eng. Mech. - ASCE,* **138**(6), 683-694.

Kahn, J.M., Katz, R.H. and Pister, K.S. (1999), “Next century challenges: mobile networking for ‘Smart Dust’”, *Proceedings of the 5th annual ACM/IEEE international conference on Mobile computing and networking*, ACM.

Kim, J., Swartz, A., Lynch, J.P., Lee, J.J. and Lee, C.G. (2010), “Rapid-to-deploy reconfigurable wireless structural monitoring systems using extended-range wireless sensors”, *Smart Struct. Syst.*, **6**(5-6), 505-524.

Kurata, N., Spencer, B.F. and Ruiz-Sandoval, M. (2005), “Risk monitoring of buildings with wireless sensor networks”, *Struct. Control Health*, **12**(3-4), 315-327.

Kurzweil, L.G. (1979), “Ground-borne noise and vibration from underground rail systems”, *J. Sound Vib.*, **66**(3), 363-370.

LAN/MAN Standards Committee (2003), “Part 15.4: wireless medium access control (MAC) and physical layer (PHY) specifications for low-rate wireless personal area networks (LR-WPANs)”, *IEEE Computer Society.*

Lee, P.J. and Griffin, M.J. (2013), “Combined effect of noise and vibration produced by high-speed trains on annoyance in buildings”, *J. Acoust. Soc. Am.*, **133**(4), 2126-2135.

Li, H., Li, X., Parriaux, A. and Thalmann, P. (2013), “An integrated planning concept for the emerging underground urbanism: Deep City Method Part 2 case study for resource supply and project valuation”, *Tunn. Undergr. Sp. Tech.*, **38**, 569-580.

Lynch, J.P., Law, K.H., Kiremidjian, A.S., Kenny, T.W., Carryer, E., and Partridge, A. (2001), “The design of a wireless sensing unit for structural health monitoring”, *Proceedings of the 3rd International Workshop on Structural Health Monitoring*.

Lynch, J.P., Sundararajan, A., Law, K.H., Kiremidjian, A.S., Carryer, E., Sohn, H. and Farrar, C.R. (2003), “Field validation of a wireless structural monitoring system on the Alamosa Canyon Bridge”, *Smart Struct. Mater*., **5057**, 267-278. *International Society for Optics and Photonics*.

Pakzad, S.N., Fenves, G.L., Kim, S. and Culler, D.E. (2008), “Design and implementation of scalable wireless sensor network for structural monitoring”, *J. Inf. Syst.*, **14**(1), 89-101.

Pitilakis, K., Tsinidis, G., Leanza, A. and Maugeri, M. (2014), “Seismic behaviour of circular tunnels accounting for above ground structures interaction effects”, *Soil Dyn. Earthq. Eng.*, **67**, 1-15.

Qin, F., Zhang, X. and Zhou, Q. (2014), “Evaluating the impact of organizational patterns on the efficiency of urban rail transit systems in China”, *J. Transport Geog.*, **40**, 89-99.

Rice, J.A. and Spencer Jr, B.F. (2009), *Flexible smart sensor framework for autonomous full-scale structural health monitoring*, Newmark Structural Engineering Laboratory. University of Illinois at Urbana-Champaign.

Ruiz-Sandoval, M., Nagayama, T. and Spencer Jr, B.F. (2006), “Sensor development using Berkeley Mote platform”, *J. Earthq. Eng.*, **10**(2), 289-309.

Sanayei, M., Maurya, P. and Moore, J.A. (2013), “Measurement of building foundation and ground-borne vibrations due to surface trains and subways”, *Eng. Struct.*, **53**, 102-111.

Sim, S.H., Li, J., Jo, H., Park, J.W., Cho, S., Spencer Jr, B.F. and Jung, H.J. (2014), “A wireless smart sensor network for automated monitoring of cable tension”, *Smart Mater. Struct.*, **23**(2), 025006.

Sugiyama, T., Maeda, K. and Kaneko, M. (1990), “Traveling wave effects on a tall and narrow building: observation and analysis”, *Comput. Geotech*., **9**(4), 307-324.

Walker, J.G. and Chan, M.F.K. (1996), “Human response to structurally radiated noise due to underground railway operations”, *J. Sound Vib.*, **193**(1), 49-63.

Widrow, B. (1956), “A study of rough amplitude quantization by means of Nyquist sampling theory”, *Circuit Theory, IRE Transactions on Circuit Theory*, **3**(4), 266-276.

Yang, Y.B. and Hsu, L.C. (2006), “A review of researches on ground-borne vibrations due to moving trains via underground tunnels”, *Adv. Struct. Eng.*, **9**(3), 377-392.

Yick, J., Mukherjee, B. and Ghosal, D. (2008), “Wireless sensor network survey”, *Comput. Netw.*, **52**(12), 2292-2330.

Zhai W.M. (2015), *Vehicle-track coupled dynamics* (volume **1**), Science Press, Beijing, China.
Zhou, G.D. and Yi, T.H. (2013), "Recent developments on wireless sensor networks technology for bridge health monitoring", *Math. Probl. Eng*., **2013**(3), 1-33.

CY